An Acad Bras Cienc (2021) 93(1): e20190651 DOI 10.1590/0001-3765202120190651
Anais da Academia Brasileira de Ciências | *Annals of the Brazilian Academy of Sciences*
Printed ISSN 0001-3765 I Online ISSN 1678-2690
www.scielo.br/aabc | www.fb.com/aabcjournal

GEOCIENCES

Analysis of future climate scenarios for northeastern Brazil and implications for human thermal comfort

RAFAELA L. COSTA, GUSTAVO M.M. BAPTISTA, HELIOFÁBIO B. GOMES, FABRÍCIO D.S. SILVA, RODRIGO L. DA ROCHA JÚNIOR & ANDERSON S. NEDEL

Abstract: A thermal comfort index for the Northeast of Brazil was analyzed for two scenarios of climatic changes, A1B and A2, for 2021-2080, and compared with the reference period 1961-1990. A technique of regionalization was applied to rainfall, maximum and minimum temperature data from meteorological stations, obtained by statistical downscaling of projections from four global climate models. The results pointed to a significant reduction of rainfall and an increase of temperature for three different climatically homogeneous subregions. Regarding the thermal comfort index, the results point to an increase in days with heat discomfort between 2021 and 2080. In the northern portion, the higher percentage of days with heat discomfort will be significant since the first half of the period under appreciation, i.e., from 2021 to 2050. Conversely, in the eastern of northeastern Brazil, the increase of days with heat discomfort should happen in the period from 2051 to 2080, whereas the central-western part of the region, which, in the reference period, had recorded less than 1% of days with heat discomfort, might see an elevation of that percentage to 7% between 2021 and 2050, potentially reaching 48% of its days made uncomfortable by heat between 2051 and 2080.

Key words: statistical downscaling, temperature, trends, Kawamura discomfort index.

INTRODUCTION

Thermal comfort can be defined as the psychological condition of an individual that expresses satisfaction regarding the thermal conditions offered by the surrounding environment. From a physiological perspective, thermal comfort happens whenever there is a thermal balance in the exchange of heat between the individual's body and the environment in the absence of regulatory sweat (Fanger 1970). Concerning physical sensations, thermal comfort is related to bodily perceptions such as very hot, hot, warm, neutral, cool, cold and very cold (Silva et al. 2018).

Climatic conditions are essential for the establishment of comfort or discomfort conditions, with a direct influence of other metabolic variables (age, nutrition, gender, ethnicity etc.), as well as the ones regarded as personal preferences, such as clothing (Givoni 1976). Extreme conditions of discomfort by heat or cold lead to serious consequences to human health, occasionally including death. Such problems have been intensified by anthropic activities that have interfered with the natural variability of the climate (Molion & Lucio 2013), due to the addition of thousands of tons of greenhouse gases to the atmosphere every year.

According to the fifth IPCC report (IPCC 2013), populations of large cities, mainly in developing

countries, tend to suffer the greatest impacts of climate change due to the effects related to public health issues. Changes in soil use and occupation, for instance, tend to increase the occurrence of extreme events associated with temperature. An example is the intensification of Urban Heat Islands (UHI), as studied by Peres et al. (2018) for the city of Rio de Janeiro, and the cases of morbidity associated with strong heatwaves (Hunt 2007, Thorsson et al. 2014, 2017).

Intense and long-lasting heatwaves have become more frequent. Trigo et al. (2005) stated that the extremely warm summer of 2003 in Europe exceeded any other in the past 500 years, while Schär et al. (2004) concluded that such an event was very unlikely to happen from a statistical point of view, when considering previous observed data, being consistent only with results of climate change simulations. Stott et al. (2004) estimated that the anthropogenic influence has doubled the possibility of the occurrence of heatwaves in Europe. More severe and frequent heatwaves for future horizons had been already predicted by Meehl & Tebaldi (2004) and Beniston (2004), based on climate change simulations.

In a recent research for the southwest of the United States (US), Guirguis et al. (2018) studied climate projections of ten CMIP5 models via Probability Density Functions (PDF) of maximum and minimum temperatures in order to determine the future likelihood of heatwaves. They reached the conclusion that the probabilities of a greater incidence of heatwaves do not directly follow the projections of future warming. However, the projected changes in the probabilities of heatwaves are explained, mostly, by an abrupt change on the daily distribution of temperatures, with places of lower projected warming expected to experience higher probabilities of heatwave occurrences, as their probability distribution functions exhibit shorter tails.

Both heat and cold waves are intimately related to imbalances on the human thermal comfort conditions. During events of severe heat, the combination of high temperatures, high levels of solar radiation and low wind speeds results in the main cause of stress due to heat as perceived by humans (Lee et al. 2013). Such an imbalance may lead to serious consequences, such as a high number of hospitalizations and, eventually, fatalities (Guo et al. 2011, 2014, Gasparrini et al. 2015a, b). Gabriel & Endlicher (2011) demonstrated that the death rate in large urban areas in Germany is higher than in rural areas.

In South America, especially with respect to the Northeast of Brazil (NEB), there is not yet a detailed research on how the recent climate variations, as well as the climate change expected for the 21st century, should affect the conditions of human thermal comfort. Usually, the NEB, as well as the whole country, rely on fragmented studies regarding the implications of climate change on this particular field of Biometeorology (Frota & Schiffer 2003, Nóbrega & Lemos 2011, Santos et al. 2012, 2014, Gobo & Galvani 2012, Costa et al. 2020).

The NEB is a very vulnerable region to climate variability from social and climatic perspectives (Vergolino & Dantas 2005, Cunha et al. 2018, Marengo et al. 2018, Martins et al. 2018, da Rocha Júnior et al. 2020). The semiarid climate prevails over the region, with high tempeartures and poor spatial-temporal distribution of rains (Salviano et al. 2016, da Rocha Júnior et al. 2019). It is the third largest region of Brazil, with a territorial extension equivalent to that of Mongolia, and it hosts about the same population as Italy. The region comprises nine states of Brazil, with approximately 72% of its population living in urban areas, and has the

lowest Human Development Index among the five Brazilian regions, of around 0.716 (on average) according to official information from the Brazilian Institute of Geography and Statistics (IBGE 2017). That index accounts for three main parameters: life expectancy at birth, gross enrolment in education ratio and gross domestic product per capita. Climate projections for the NEB indicate that, until the end of the 21st century, the region should see an average increase of 2°C to 4°C in maximum and minimum temperatures, according to the most pessimistic scenarios, or an elevation of around 1°C to 3°C in accordance with the most optimistic ones, as well as an overall significant reduction in rainfall (Chou et al. 2014, Franchito et al. 2014, Marengo et al. 2016).

In view of all that, the aim of this work is to fulfil two major gaps in the research field related to the climate of the NEB and the impacts of climate change on the region: to verify the quality of climate projections for the NEB via statistical downscaling – a novelty for this particular region, given that traditional approaches have always employed techniques of dynamic downscaling (Sales et al. 2015, Guimarães et al. 2016) – for the observed reference climate (1961-1990) and for two future scenarios of climate change, A1B (considered realistic) and A2 (regarded as pessimistic), both from the fourth IPCC report (IPCC 2007), for the 2021-2080 horizon (split in two halves: 2021-2050 and 2051-2080). Then, the second goal will be to analyse the thermal comfort for the same climate reference and for future conditions. For the generation of regionalized climate scenarios, the Statistical DownScaling Model (SDSM) technique will be applied to the projections of four Global Climate Models (GCMs), in order to synthetize time series of rainfall and temperature for 97 weather stations spatially distributed along the NEB. For the thermal comfort index, we resort to the one proposed by Ono & Kawamura (1991), a dimensionless mathematical expression recommended for intertropical regions, which takes into account the air temperature and relative humidity (represented in the equation by the dew point temperature), being applicable to dressed adult people at rest and submitted to a slight motion of the air (Sampaio et al. 2018).

MATERIALS AND METHODS

Area of study and observed data

According to official information from IBGE (2017), the NEB occupies 18.27% of the Brazilian territory, with an area of approximately 1,558,000 km², being the third largest of the five Brazilian regions. The region comprises nine states of the Federation (Figure 1a). Observed rainfall data (PRCP), maximum temperatures (TX), minimum temperatures (TN) and relative humidity (RH) from 97 weather stations, installed and managed by the National Meteorological Institute of Brazil (INMET, acronym in Portuguese), located in the NEB (Figure 1b), from 1961 to 2000, are used to characterize the climatology of the region for the purpose of detecting climatically homogeneous regions (Costa et al. 2020), as well as to calculate the KDI thermal comfort index (Ono & Kawamura 1991), and to serve as a parameter for calibrating (1961-1990) and validating (1991-2000) the SDSM used to generate future climate scenarios.

Kawamura discomfort index (KDI)

The calculation of the KDI is based on the average ambient temperature (T, in °C) and the dew point (Td, in °C), which is a function of the Relative Humidity (RH), given that it is the temperature at which water vapor condensates. The KDI can be obtained by the following Equation 1:

$$KDI = 0,99T + 0,36T_d + 41,5 \quad (1)$$

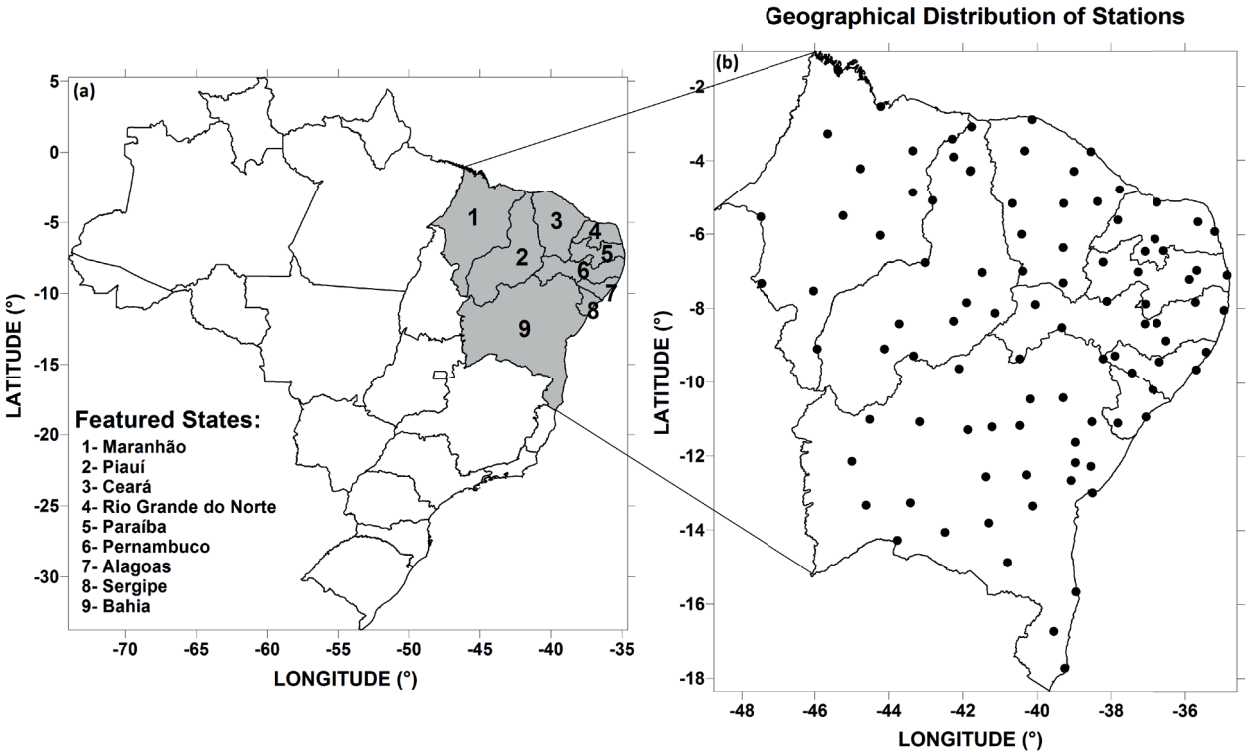

Figure 1. Map of Brazil highlighting the Northeast region (NEB) in gray, with numerically identified states (a), and the distribution of the 97 meteorological stations (b).

Td is calculated empirically from daily data of a conventional weather station by relating T and RH through Equation 2:

$$T_d = T - (14,55 + 0,114 \times T)(1 - (0,01 \times RH)) - \left((2,5 + 0,007 \times T)(1 - (0,01 \times RH))\right)^3 - (15,9 + 0,117 \times T)(1 - 0,01 \times RH)^{14} \quad (2)$$

The use of that index makes it possible to determine conditions of comfort, discomfort or stress due to cold or heat as felt by the population, in accordance with the intervals proposed by Ono & Kawamura (1991), presented in Table I.

Climate scenarios

The future climatic scenarios of PRCP, TX and TN were built for the NEB using SDSM from four outputs of GCMs: ECHAM5-OM, from the Max Planck Institute for Meteorology, Germany (Marsland et al. 2003, Raddatz et al. 2007); HadGEM2-ES, Met Office Hadley Centre, UK, (Bellouin et al. 2007, Collins et al. 2008); BCM, version 2, The Bjerknes Centre for Climate Research, University of Bergen (UiB), Norway; and CNRM-CM3, from Centre National de Recherches Météorologiques, France. For the purpose of regionalization, the A1B and A2 scenarios were used, both of them from the fourth IPCC report (IPCC 2007). The A1B scenario represents a realistic horizon, with fast economic growth by intensive use of fossil fuels and little interest in sustainability processes, although mankind will seek a balance with clean energy sources. The A2 scenario describes a very heterogeneous world. The underlying theme is self-reliance and preservation of local identities. Fertility patterns across regions converge very slowly, which results in continuously increasing global population. Economic development is primarily

Table I. KDI classification.

KDI Values	Thermal sensation
KDI ≥ 80	Stress due to heat
75 ≤ KDI < 80	Heat discomfort
60 ≤ KDI < 75	Comfortable
55 ≤ KDI < 60	Cold discomfort
KDI < 55	Stress due to cold

regionally oriented and per capita economic growth and technological change are more fragmented and slower (Raskin et al. 2005, SRES 2010).

The SDSM (Wilby et al. 2002) is a downscaling tool that enables low cost and fast growth projections of climate variables measured by surface weather stations under current and future climate forcings. It combines information from GCMs with reanalysis data for the same grid spacing, in order to identify and select the best large scale predictors for the surface variables. In that regard, several authors suggest, as good predictors, variables that represent atmospheric circulation, such as sea level pressure (SLP), Geopotential Height (GPH), zonal and meridional wind components, temperature and humidity at different atmospheric levels, among others (Wilby & Wigley 1997, Wilby & Dawson 2004, 2013, Timbal & Jones 2008, Maraun et al. 2010).

For the present research, from a partnership celebrated with the University of Cantabria as part of the activities of Project ENSEMBLES, funded by the European Union (Cofiño et al. 2007), the functionalities provided by the software developed by the Santander Meteorology Group (http://www.meteo.unican.es) were used to obtain the SDSM. Downscaling with SDSM results from three main steps: (a) selection of predictants and predictors, (b) selection of SDSM and (c) generation and validation of scenarios (Wilby & Fowler 2010), as detailed in the following sections.

Selection of predictors and predictants

There are several ways to characterize the climate of a region from a set of selected predictors. In this research, the analogues method was used as a transfer function (Carter 2007, Kopf et al. 2008, Ishizaki et al. 2012). The choice of predictors should be based on the physical knowledge of the variables that regulate the average climatic conditions of the region and exert a strong influence on the daily temperature, humidity and rainfall occurrence (Cavalcanti & Mariano 2016, Alves et al. 2017). ERA40 reanalysis data were used for calibration of rainfall, and NCEP/NCAR data, for calibration of maximum and minimum temperatures in a 2.5° x 2.5° common grid for the 1961-1990 control period (Flato et al. 2013, Hartmann et al. 2013).

For PRCP, TX and TN, the following predictors were used: zonal and meridional components of the average wind velocity at the 850 hPa level, specific humidity at the 850 hPa level, mean sea level pressure, geopotential height at 500 hPa and temperature at the 850 hPa level. The predictability of the model based on the analogue method is also influenced by the number of variables used. Too many predictors may increase model noise and, therefore, lead to a decrease in predictive power. On the other hand, few predictors can neglect valuable information (Wilks 2011).

The predictants are PRCP, TX and TN, whose time series were entered in the ENSEMBLES Downscaling Portal database.

Selecting SDSM

The SDSM we resorted to was the analogue method (Gutiérrez et al. 2013), considering that it presents the best correlations for most stations when compared to other available methods,

such as linear regression and artificial neural networks. In this method, analogous patterns are filtered by Empirical Orthogonal Functions (EOFs), specifying a local state consistent with a simultaneous large-scale state (Van den Dool 1994, Zorita et al. 1995, Zorita & von Storch 1999). As an example, the atmospheric circulation anomalies represented by (f) of the SLP field are described by few major EOFs patterns:

$$f\left(i,t\right)=\sum_{k=1}^{n}xk_{t}gk_{i}+\varepsilon_{t} \quad (3)$$

where *i* is a grid point index, *t* is time, *gk* is the k-order pattern of the EOF, *xk(t)* is the amplitude of this standard at time *t*, *n* represents the number of EOF patterns retained, and Є is the part of the variability not described by the major standards *n*, considered small. Analogs are only searched within the space generated by these standard nodes.

Generation of scenarios and validation

Future scenarios were generated for the period 2021-2080, split in two distinct periods of 30 years (2021-2050 and 2051-2080) for comparison with the observed reference climatology 1961-1990. In addition to these scenarios, the time series of the variables for the period 1961-2000 were reconstructed for each model, in order to assess how well they represent the observed climatology, with data from the period 1961-1990 (75% of the data) being used to evaluate the similarity of the simulated climate with the observed SDSM, and data from 1991-2000 (25% of the data), being used for validation. This is one of the most important steps, i.e., comparing the daily data observed and simulated in this period, in order to demonstrate the models' ability in simulating the past climate, which grants confidence for future climate analysis. Several statistical parameters are obtained for rainfall and temperature, such as: Pearson correlation coefficient (r), PDFescore, variance ratio, absolute and quadratic mean errors, BIAS and comparisons of the differences between means, medians and standard deviations obtained from simulated and observed series. The t-student statistical significance test was used to obtain the critical correlation value (rc), a value that allows us to assume the statistical hypothesis that there is a correlation between the simulated and observed data at a statistical confidence level of no less than 95% (Berthouex & Brown 2002).

KDI scenarios

In order to calculate the KDI, it is necessary to know T and Td. T is obtained from the simple average of TX and TN, while Td comes from T and RH through Equation 2. However, considering that the downscaling process provides results solely for PRCP, TX and TN, we found out that it is possible to obtain RH values that are much closer to the observed ones by resorting to Multiple Linear Regression (MLR), with PCRP, TX and TN being used as predictors for RH.

The smooth nature of the data and the inversely proportional relationship between temperature and humidity makes it safe to imply that one variable responds well to the mean daily behaviour of the other, and vice-versa. The PRCP, being of a random and zero-inflated nature, exhibits a much lower predictive potential than the ones of TX and TN, with a verified importance in the representation of RH limited to rainy days.

The MLR was applied to the period of observed data (1961-1990). Such new values of RH were used to derive the respective Td values (Equation 2). The comparison between the observed and modelled RH and Td data sets proved the method to be satisfactory, with high values of correlation (r), low values of BIAS and of Root Mean Square Error (RMSE). Finally, those equations were applied

to the PRCP, TX and TN scenarios, allowing for the calculation of the variables necessary to obtain the KDI (Equation 1).

Regionalization of results

The climate of the NEB is conditioned by the performance of several meteorological systems and different modes of variability, which operate at different times of the year. The rainy period in the northern NEB is marked by the action of the Intertropical Convergence Zone (ITCZ) and Upper Tropospheric Cyclonic Vortexes (UTCV) during the austral summer and early autumn. The rainy season in the eastern sector and part of the central portion is marked by the action of UTCVs and the propagation of Easterly Wave Disturbances (EWDs) coming from the Atlantic Ocean during the months May–June–July (MJJ). UTCVs and Cold Fronts are the main rain generators in the southern sector of the NEB during the austral summer, and EWDs, during autumn/winter. The most central area of the NEB has its rainy season concentrated in the months of November-December-January (NDJ), due to the South Atlantic Convergence Zone (SACZ) (Kousky 1979, Kousky & Gan 1981, Costa et al. 2014, Cordeiro et al. 2018, de Carvalho et al. 2013, Silva et al. 2013, Gomes et al. 2015, 2019). Some modes of variability modulate the rainfall over the NEB, with low temporal frequency, such as the North Atlantic Oscillation, the Pacific Decadal Oscillation, the Atlantic Multidecadal Oscillation and the Madden-Julian Oscillation (Servain 1991, Servain et al. 2000, Kousky & Kayano 1994, Kayano & Andreoli 2004, Kayano & Capistrano 2014). The influence of different systems in this vast region require a subdivision into three major climatic areas, as in Costa et al. (2020). The determination of those subregions was achieved by employing a hierarchical cluster analysis to the PRCP, TX and TN data sets, adopting the Euclidian distance as a measure of similarity (Mimmack et al. 2001, Costa et al. 2020) and, for the clustering algorithm, we used the Ward Method. This method, according to the literature (Hervada-Sala & Jarauta-Bragulat 2004), identifies the smallest variation among clusters, grouping elements whose sum of squares is minimal, or whose sum of errors is minimal, using an unsupervised method known as K-media (André et al. 2008), whose objective is to group the experimental units according to the similarity between them, in this case, areas of the same climatic characteristics.

RESULTS AND DISCUSSION

In this section, we describe the analysis performed to assess the potential changes in the mean KDI pattern for the three NEB subregions when submitted to future scenarios of regionalized climate change. First, a climate assessment with observed data is performed in order to characterize the three subregions. Next, we show the ability of the models to simulate the current climate, its virtues and deficiencies, through the analysis of the calibration process and validation of the employed SDSM technique. Then, the profiles of changes in the environmental variables under each of the future scenarios, necessary to obtain the KDI, are analyzed for each subregion and, finally, the possible changes in the average KDI standards are discussed for the respective scenarios.

Subregional climate analysis of the NEB

The cluster analysis applied to the rainfall and temperature series allowed to identify three large climatically homogeneous areas in the NEB (Figure 2a). Next, single time series for each variable of each homogenous area were obtained from the respective average values of the stations that represent them, in order to

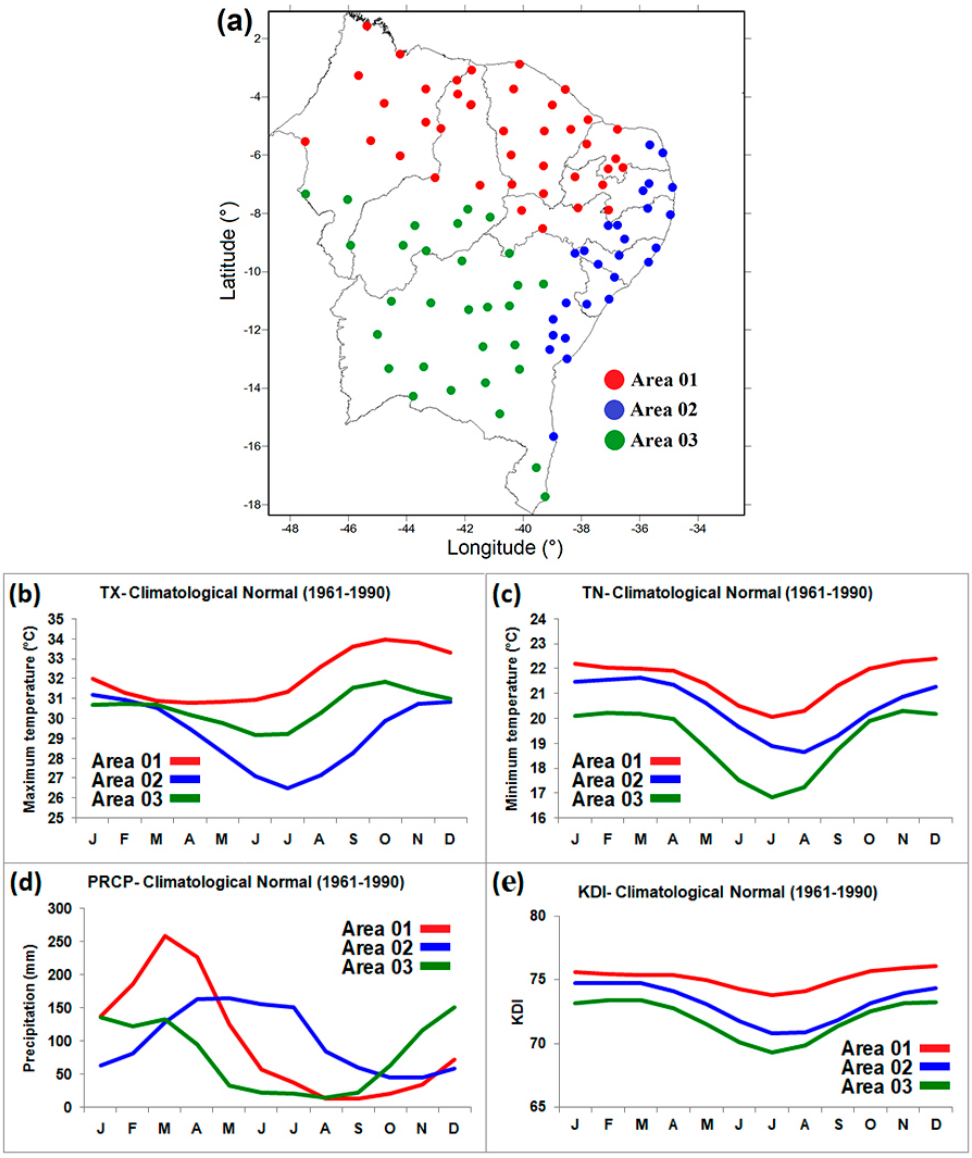

Figure 2. (a) Spatial distribution of the stations and identification of the three large areas (climate subregions), separated by color, (b) climatology observed in 1961-1990 for TX in each area, (c) the same as b, but for TN, (d) the same as b, but for PRCP and (e) the same as b, but for KDI.

point out the differences between those three subregions, as well as to enable the KDI analysis for the future scenarios of climate change. The climatology from the observed data (1961-1990) shows the distinctions in the behavior of the variables along the three areas. TX (Figure 2b) and TN (Figure 2c) are highest in Area 01, the northern NEB. During the summer, the TX values are close to, in average, the ones expressed by Areas 02 and 03, but are distant for the winter period, with Area 03 (the NEB's interior) showing higher maximums than Area 02 (eastern NEB), an expected effect of the different distances to the ocean, which results in a greater thermal amplitude in the interior. For TN, the opposite effect is observed, as a smaller thermal amplitude near the ocean imposes higher TN values for Area 02 than for Area 03.

The PRCP (Figure 2d) shows three rainfall regimes with different characteristics. There is similarity in the rainy season of Areas 01 and 03, with a minimum at the end of winter and a maximum from the end of spring and during the summer months in Area 03, and a pronounced maximum at the end of summer and beginning of autumn in Area 01.

The mean annual KDI systematically shows values in a decreasing fashion from Areas 01 to 03 (Figure 2e). The lower thermal amplitude (difference between TX and TN) in Area 02 is a determinant factor for the overall exhibition of a higher KDI than in Area 03 for most of the year. As for Area 01, the cooling that PRCP provides to the environment is a decisive factor in mitigating the effects of high temperatures in that sector, which, otherwise, would exhibit a greater distance between its average curve of KDI and those of the others (Areas 02 and 03), especially for the first half of the year.

SDSM - calibration and validation

The main objective of the SDSM calibration is to obtain a model that can accurately reflect the observed climate variability, increasing the confidence in the time series generated for the future. Figure 3 shows the capacity of the individual models (A-BCM2 model, B-CNRM-CM3 model, C-ECHAM5-OM model, D-HadGEM2-ES model), as well as the ensemble (the average of all the models, E), to reproduce the seasonal means of PRCP, TX and TN of the representative quarters of each season (DJF-summer, MAM-autumn, JJA-winter and SON-spring).

Regarding the rainfall variable, the models and the ensemble show seasonal climatological patterns similar to the observed climatology (Figure 3a). Figure 3b shows, for each season, where the models tend to overestimate/underestimate the average rainfall observed. For DJF, which is an important rainy period on the western NEB, denoted by stations within Areas 01 and 03, the models tend to underestimate the precipitation. Conversely, they exhibit a propensity to overestimate the rainfall on the eastern strip of the NEB (mostly represented by Area 02), where, according to its observed climatology, the rainy season is still a couple of months afar. Such overestimation is particularly noticeable in ECHAM5-OM (Model C). For MAM, the main rainy season in the northern NEB, the models show a very similar behavior (among them), by underestimating the northern NEB rains and overestimating the ones in the southern NEB. (Bombardi & Carvalho 2009) showed that the models, since CMIP3, have problems in the correct representation of the physical processes associated with rainfall resulting from the ITCZ, the main precipitation induction system for the northern NEB and strongly influenced by the sea surface temperature gradient of the Tropical Atlantic Ocean. JJA is the main rainy season in the eastern NEB, which corresponds to Area 02, and the driest period for the interior part of the NEB, which is represented by Area 03. For such quarter of the year, all the models tend to overestimate rainfall throughout the NEB. During the next transition season (SON), an opposite gradient to that observed for MAM prevails, with a tendency to overestimate rainfall in the northern part of the NEB, and to underestimate it in the southern region (as well as some of the western range).

The results for the rainfall variable show a great similarity among the models, with an alternation of periods and areas that exhibit a propensity to over/underestimate the precipitation, indicating the efficiency of the calibration process by the SDSM, with the same predictors being used for all the models.

TX and TN presented more satisfactory results regarding the representation of the annual cycle (Figure 3c and 3e). In Figure 3d, there was a slight overestimation of the mean values

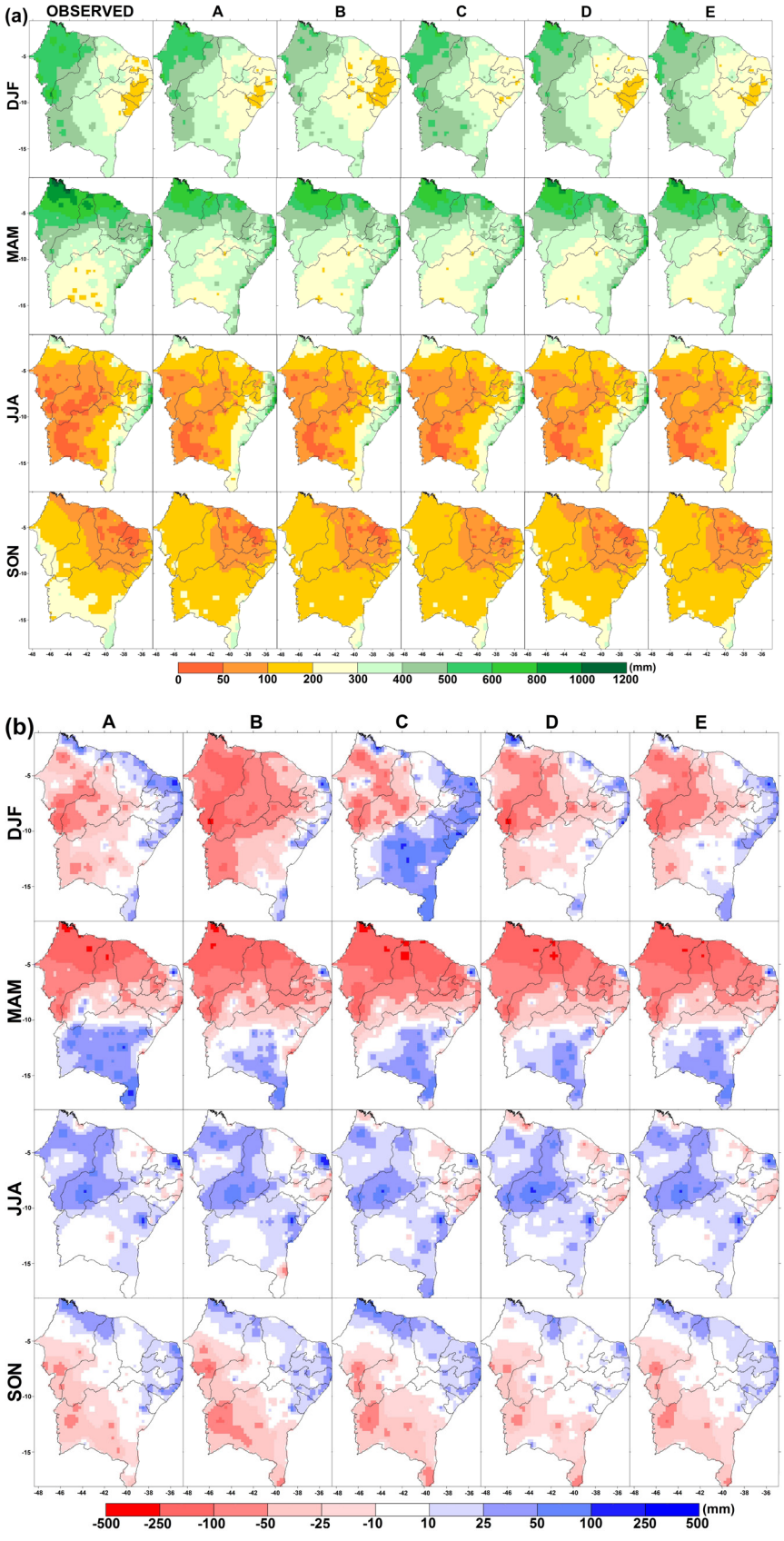

Figure 3. (a) Seasonal means of observed rainfall and the ones reproduced by each model and the ensemble for the period 1961-1990 (A-BCM2, B-CNRMCM3, C-ECHAM5-OM, D-HadGEM2-ES, E-ENSEMBLE), **(b)** deviations of each model for rainfall, **(c)** the same as a, but for maximum temperatures, **(d)** the same as b, but for maximum temperatures, **(e)** the same as a, but for minimum temperatures and **(f)** the same as b, but for minimum temperatures.

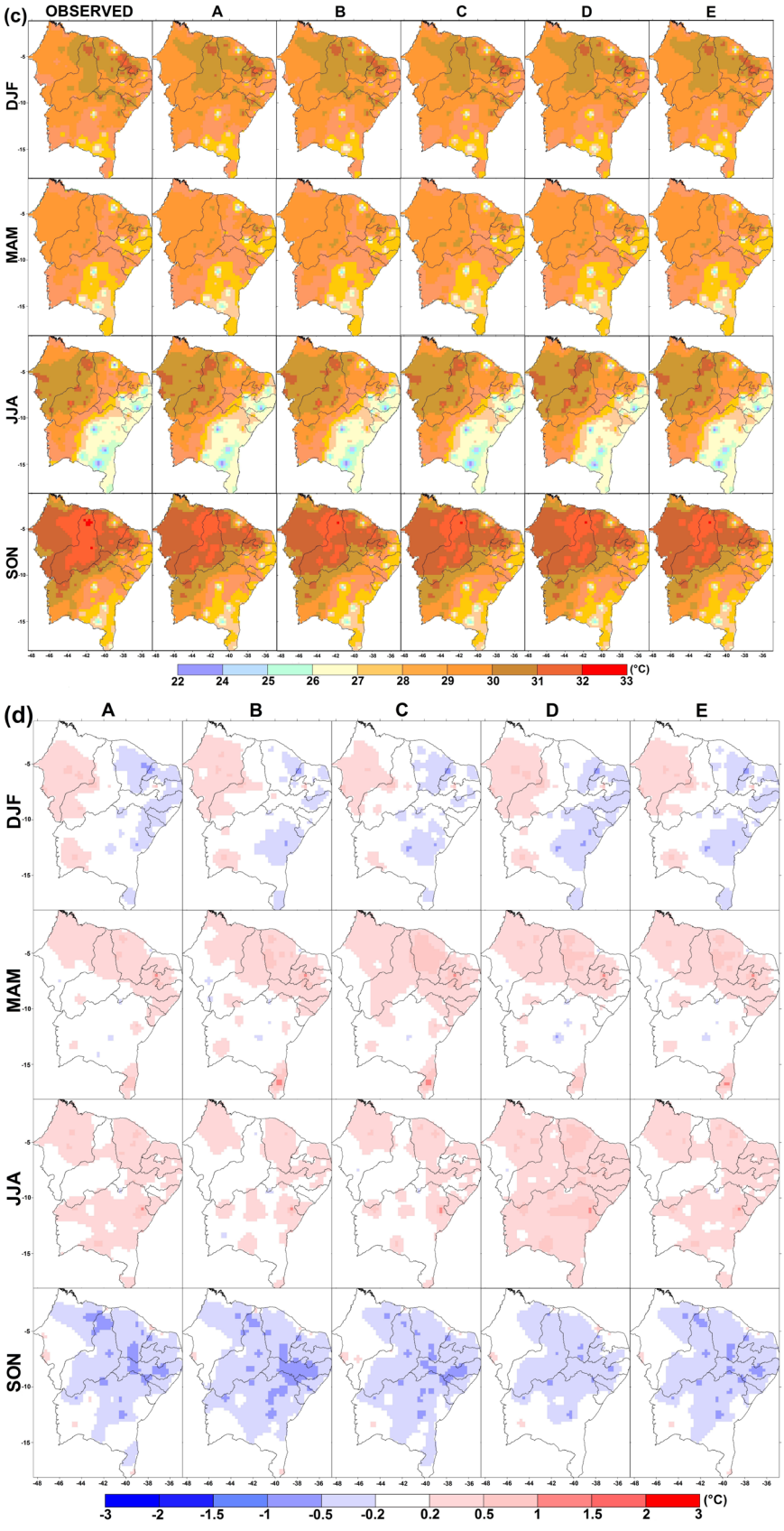

Figure 3. (a) Seasonal means of observed rainfall and the ones reproduced by each model and the ensemble for the period 1961-1990 (A-BCM2, B-CNRMCM3, C-ECHAM5-OM, D-HadGEM2-ES, E-ENSEMBLE), **(b)** deviations of each model for rainfall, **(c)** the same as a, but for maximum temperatures, **(d)** the same as b, but for maximum temperatures, **(e)** the same as a, but for minimum temperatures and **(f)** the same as b, but for minimum temperatures.

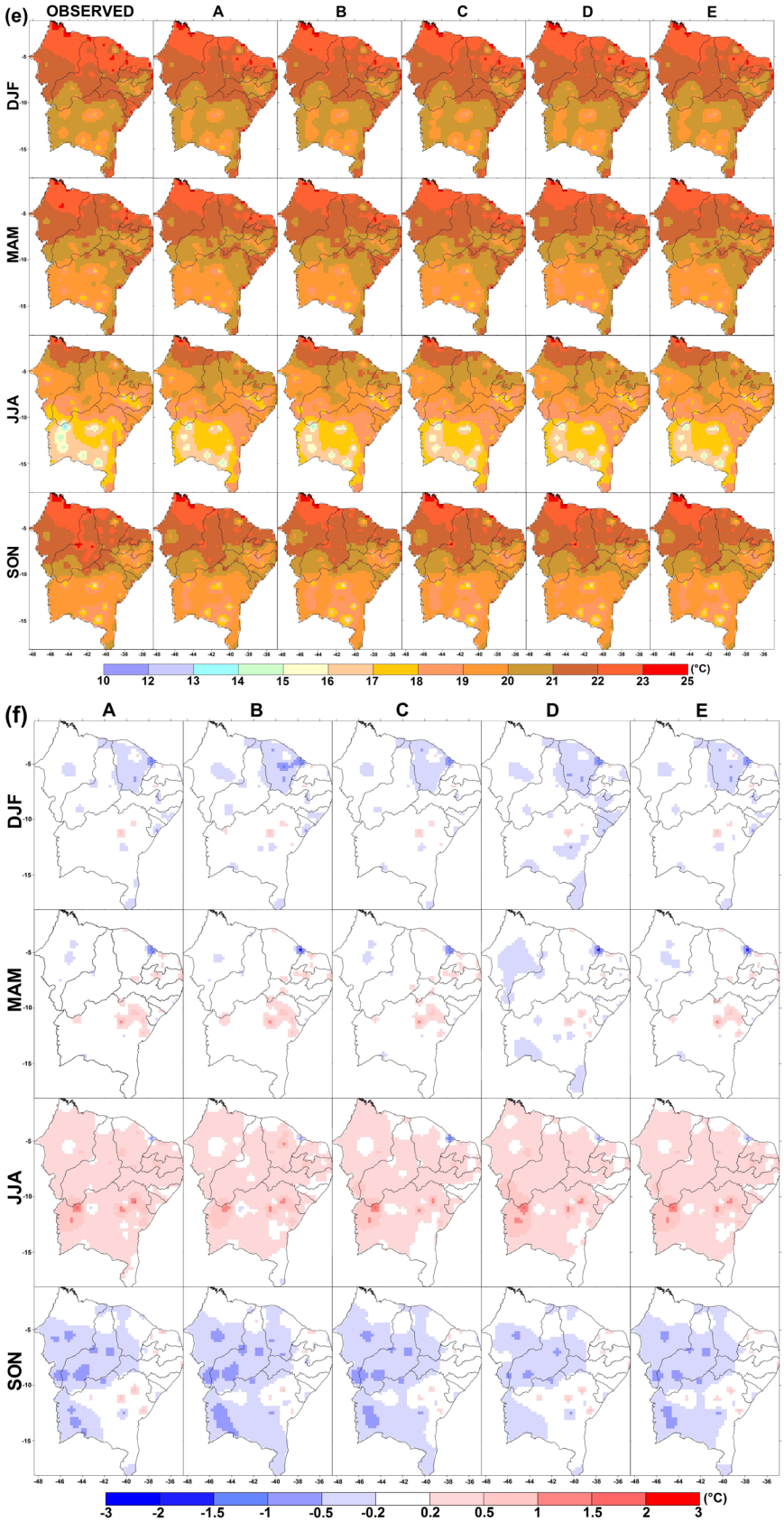

Figure 3. (a) Seasonal means of observed rainfall and the ones reproduced by each model and the ensemble for the period 1961-1990 (A-BCM2, B-CNRMCM3, C-ECHAM5-OM, D-HadGEM2-ES, E-ENSEMBLE), **(b)** deviations of each model for rainfall, **(c)** the same as a, but for maximum temperatures, **(d)** the same as b, but for maximum temperatures, **(e)** the same as a, but for minimum temperatures and **(f)** the same as b, but for minimum temperatures.

of TX in the western NEB for DJF, as well as in the northern NEB and the center-east area during MAM. The models presented average values close to those observed, with a slight overall tendency to overestimate TX. That is valid especially for the model HadGEM2-ES (D) during JJA. For SON, there was an underestimation throughout the center-east of the NEB. The TN deviations (Figure 3f) are more pronounced during JJA and SON, with patterns that resemble the ones of TX (Figure 3d), having DJF and MAM showing small nuclei alternating the behaviors of under and overestimation in relation to the observed means.

Comparing the deviations of PRCP (Figure 3b) to those of TX (Figure 3d) and TN (Figure 3f), there is a much greater distance between the simulated and the observed PRCP climatology, with areas exhibiting discrepancies greater than or equal to 100 mm, whereas, for TX and TN, the most pronounced deviations are limited to about ± 1°C.

Figure 4 depicts the validation of RH and Td data for the period 1991-2000, obtained through the MLR equations applied to the observations from the period 1961-1990, with observations from the same period. The spatial layout of the BIAS, Pearson correlation (r) and RMSE are shown.

The BIAS values for RH (Figure 4a) show a few random points of very low positive and negative values, whereas the ones for Td (Figure 4b) indicate a trend of underestimation of the observed values. The values of r were high and statistically significant concerning the comparison between simulations and observations of both variables (Figure 4c and 4d). The RMSE shows maximum errors of up to 10% between simulated and observed RH and up to 3°C for Td (Figure 4e and 4f). These parameters show acceptable patterns of comparison between the simulated and observed data, providing confidence for the use of the equations found to obtain Td and KDI from the time series of PRCP, TX and TN in the future scenarios.

SDSM - Future scenarios of climate variables

Figure 5 (top row) displays the observed climatology (Obs) of rainfall (1961-1990) and the projected future changes (2021-2050 and 2051-2080), throughout the annual cycle for the three areas determined before (Figure 2a). The decrease in rainfall is widespread and stronger in the period 2051-2080 than in 2021-2050. Over the three areas, this decrease is more significant in the rainy months of the year for each one: in Area 01, mainly between February and April, a period whose rainfall is associated with the southward displacement of the ITCZ (Moura & Shukla 1981, Kousky & Gan 1981, Zagar et al. 2011). In Area 02, the reduction indicated by the scenarios should occur with greatest intensity from March to June, a period in which the rainfall is mostly modulated by the incursion of EWD (Gomes et al. 2015, 2019). In Area 03, the most pronounced reduction in rainfall is expected to happen between October and March. Regarding annual totals, the reductions projected according to Scenario A1B for Areas 01, 02 and 03 during the period of 2021-2050 are of 215.6, 161.3 and 232.2mm, respectively, and, for 2051-2080, the expected declines are of 400.7, 351.8 and 411.6mm, also respectively to Areas 01, 02 and 03.

TX (Figure 5, middle row) show distinct behaviors of the future projections for the three areas. In Area 01, the forecast is for a more intense increase in the first half of the year, reducing the seasonal amplitude; in Area 02, the raise should occur almost equally for nearly the entire year, but more pronouncedly from May to August and, less noticeably, from October to February in 2021-2050; in Area 03, the rise should prevail for all over the year, with a lower increase in 2051-2080 from June to September compared to the increment projected from the reference period to 2021-2050. In annual terms, the projected increases according to scenario A1B for Areas 01, 02 and 03 during 2021-2050 are of 0.7, 0.7 and

1.1°C, and, for the period 2051-2080, the maximum temperatures should raise by 1.1, 1.6 and 2.2°C, respectively.

TN is the variable that exhibits the most homogeneous behavior throughout the three areas (Figure 5, bottom row). In annual terms, the projected increases conforming to scenario A1B for Areas 01, 02 and 03, over the period 2021-2050, are of 0.7, 0.8 and 0.7°C, and, for the period 2051-2080, the minimum temperatures may be elevated by 1.5, 1.8 and 1.7°C, respectively. The same analysis, for the three variables, was made for scenario A2 (not shown), whose results were very similar, in behavior and values, to those obtained for scenario A1B.

KDI, observations and projections

Figure 6 features the comparison of KDI histograms relative to the daily data obtained from the observations (1961-1990) and the average of the models, for the three climatologically homogeneous areas of the NEB. In all the cases, no circumstances of stress and discomfort due to cold were identified. For Area 01 (Figure 6a and 6b), the models overestimated the KDI class range from 75 to 80, which represents heat discomfort, underestimating the comfortable range. For Area 02 (Figure 6c and 6d), the model reproduced the observations with better accuracy, slightly underestimating the comfortable range and also just marginally overestimating the range of heat discomfort. For Area 03 (Figure 6e and 6f), the average of the models virtually eliminated the comfort range from 65 to 70, presenting nearly all of their values within the comfort range, between 70 and 75. Overall, the models represented well the observed conditions.

Next, we present the KDI results of the models' average for scenarios A1B and A2 concerning the periods 2021-2050 and 2051-2080, in order to better understand which of them will make a greater contribution to the changes in the daily behavior according to the models. Figure 7, for Area 01, shows scenarios of significant reduction in days classified as comfortable, that is, that have a KDI between 60 and 75. Under scenario A1B, for 2021 to 2050 (Figure 7a), 7.3% of the days will be considered comfortable and 92.7%, uncomfortable by heat, this percentage decreases slightly in scenario A2 (Figure 7b), to 91.8% of days causing heat discomfort and 8.2% considered comfortable. For the period 2051-2080, in accordance with scenario A1B (Figure 7c), 98.6% of the days will be uncomfortable by heat, with only 1.4% being regarded as comfortable. For scenario A2 (Figure 7d), 97.9% of days are expected to be uncomfortable by heat, and 2.1%, comfortable.

Figure 8 demonstrates that Area 02 should have more days classified as comfortable (56.1%) than with heat discomfort (43.9%) during 2021-2050 according to scenario A1B (Figure 8a), with similar numbers being delivered by scenario A2: 55.4% of comfortable days and 44.6% of heat-discomfort days (Figure 8b). The period 2051-2080 should see a reversal in those circumstances, with the predominance of days with discomfort by heat for both scenarios: 68.5% of days for scenario A1B (Figure 8c) and 68.9% for scenario A2 (Figure 8d). Figure 9 shows an increase in the percentage of days with discomfort by heat of the order of 7.7% for the period 2021-2050 for Area 03, conforming to scenario A1B (Figure 9a), and of 6.9%, for scenario A2 (Figure 9b). Those percentages might increase significantly for the period 2051-2080, reaching 48.1% of the days with discomfort by heat for scenario A1B (Figure 9c) and 47.2% for scenario A2 (Figure 9d). It should be noted that, during 1961-1990, the number of observed days with discomfort by heat did not exceed 1% (Figure 6e), and that the models did not even simulate any days with heat discomfort (Figure 6f).

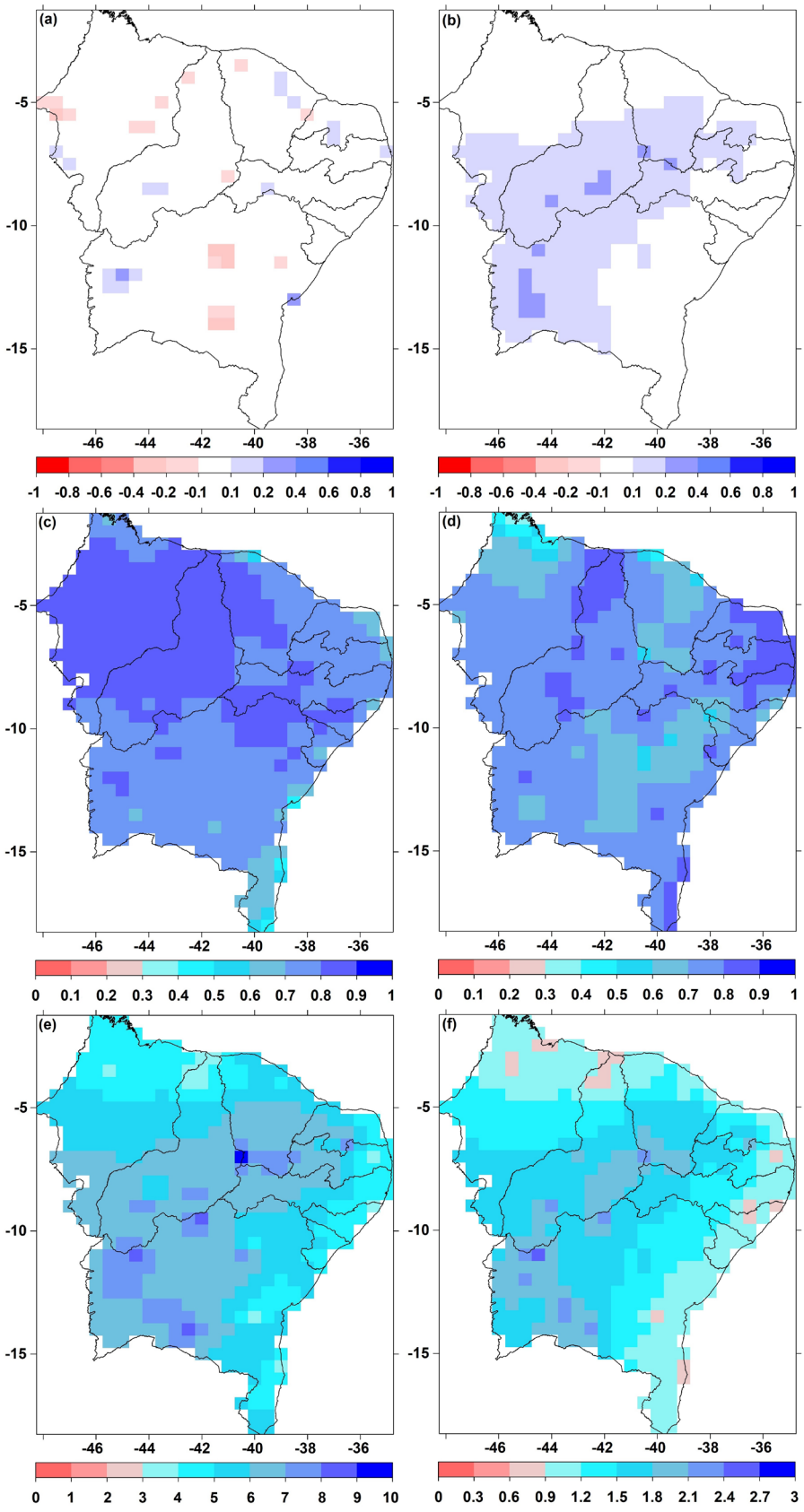

Figure 4. (a) Bias between simulated and observed RH, **(b)** Bias between simulated and observed Td, **(c)** correlation r between simulated and observed RH, **(d)** correlation r between simulated and observed Td, **(e)** RMSE between simulated and observed RH, and **(f)** RMSE between simulated and observed Td. Statistical parameters obtained for the validation period of the SDSM: 1991-2000.

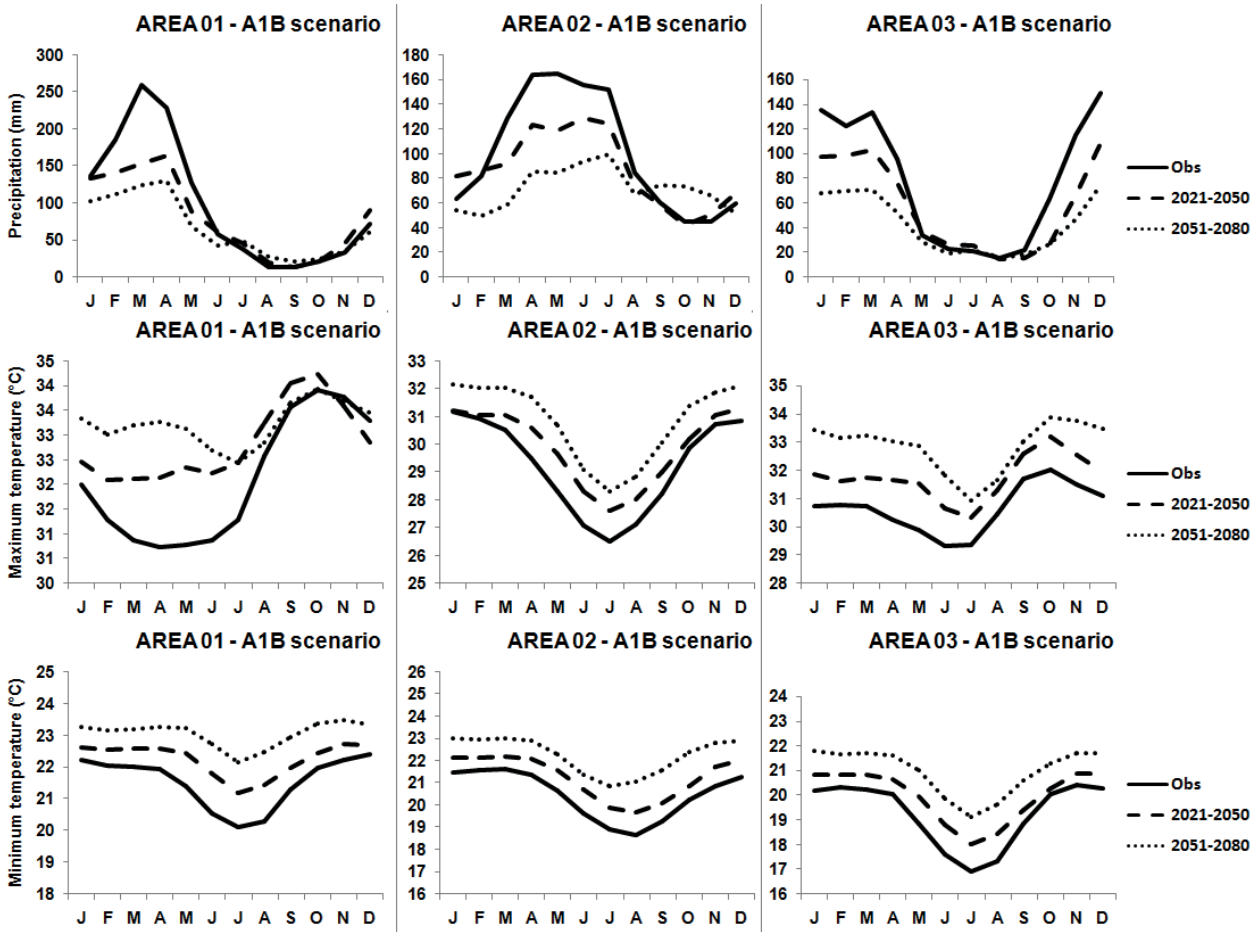

Figure 5. here *top row* **Observed annual cycle of rainfall (Obs, 1961-1990) and projected future changes for the three areas over the two periods of time (2021-2050 and 2051-2080),** *middle row* **The same as in the** *top row*, **but for monthly averaged for maximum temperature,** *bottom row* **The same as in the top row, but for monthly averaged minimum temperature.**

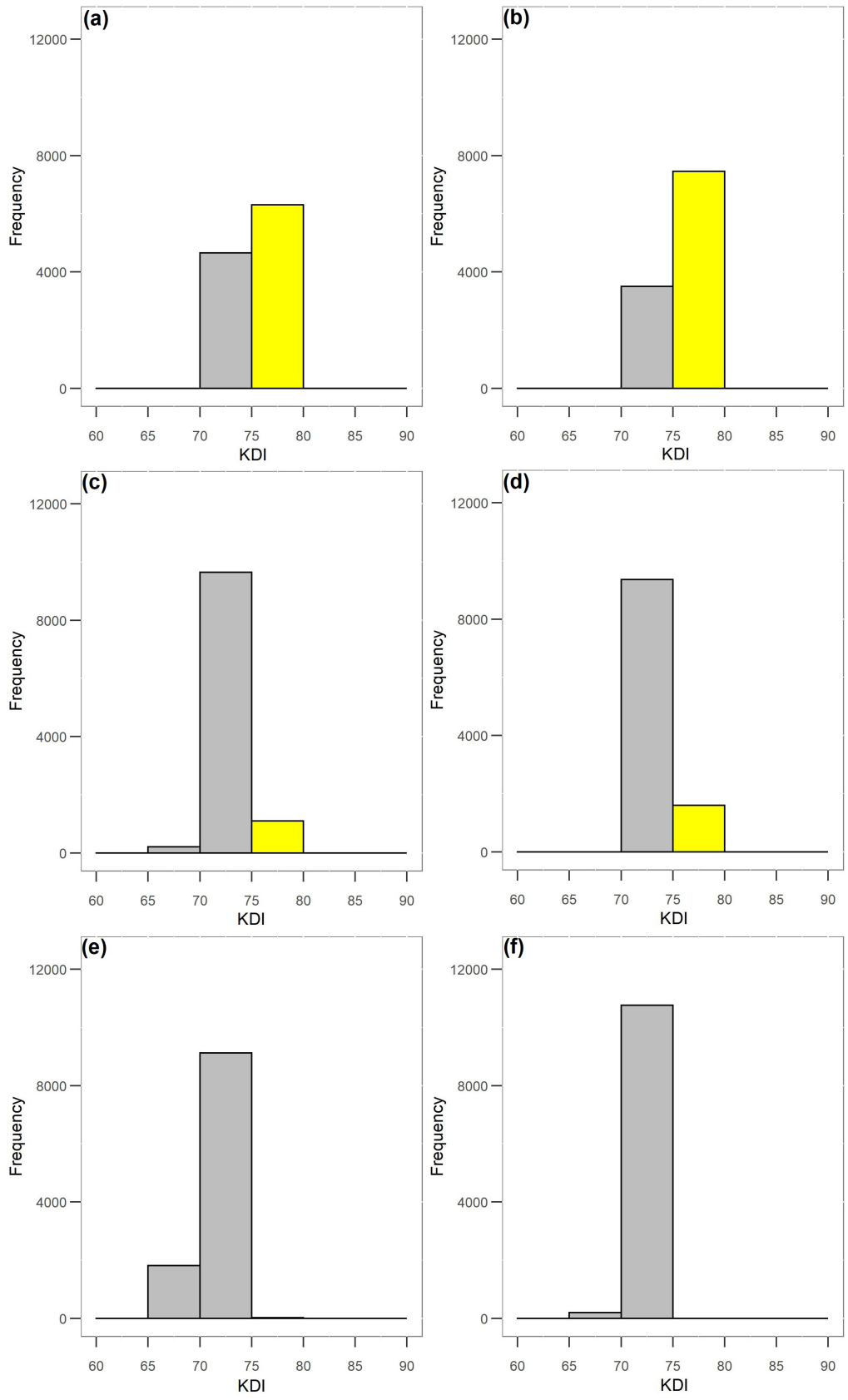

Figure 6. Histograms of the daily log of observations **(a)** and simulations **(b)** from the average of the KDI models for the period 1961-1990 for Area 01, for Area 02 **(c)** and **(d)**, for Area 03 **(e)** and **(f)**. The gray color indicates the comfortable range, while yellow represents the uncomfortable range by heat.

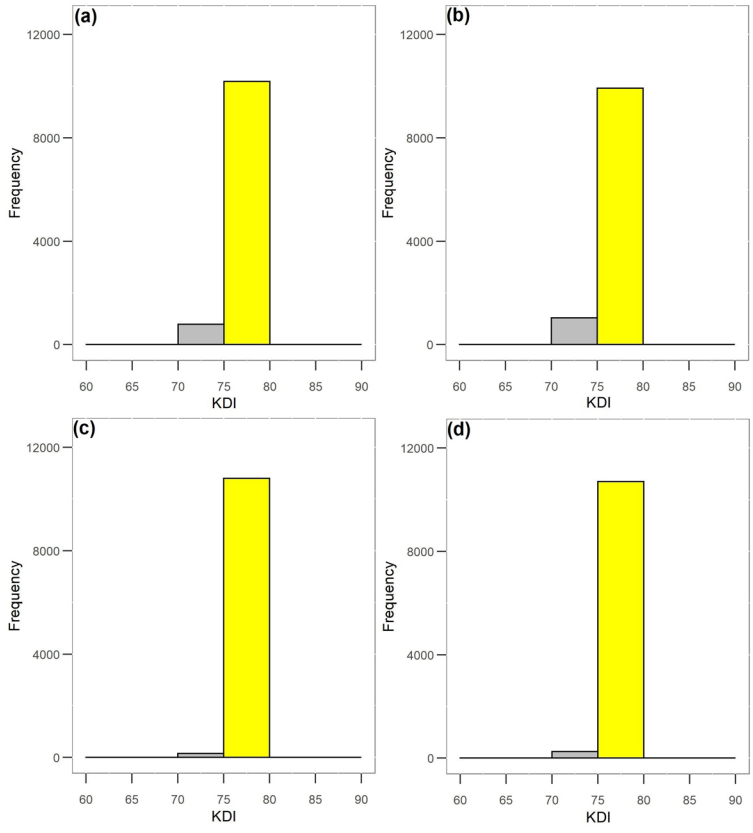

Figure 7. Histograms of the future scenarios of the daily KDI classification for the periods 2021-2050 according to scenarios A1B **(a)** and A2 **(b)**, and 2051-2080 for scenarios A1B **(c)** and A2 **(d)**, from the results of the models for Area 01. The gray color indicates the comfortable range, while yellow represents the uncomfortable range by heat.

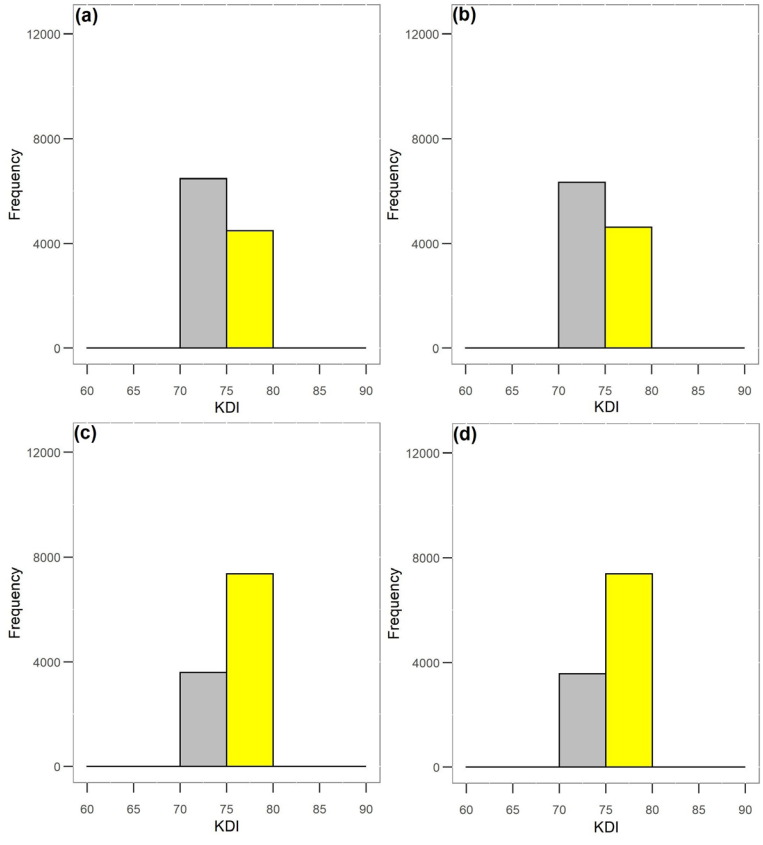

Figure 8. Histograms of the future scenarios of the daily KDI classification for the periods 2021-2050 according to scenarios A1B **(a)** and A2 **(b)**, and 2051-2080 for scenarios A1B **(c)** and A2 **(d)**, from the results of the models for Area 02. The gray color indicates the comfortable range, while yellow represents the uncomfortable range by heat.

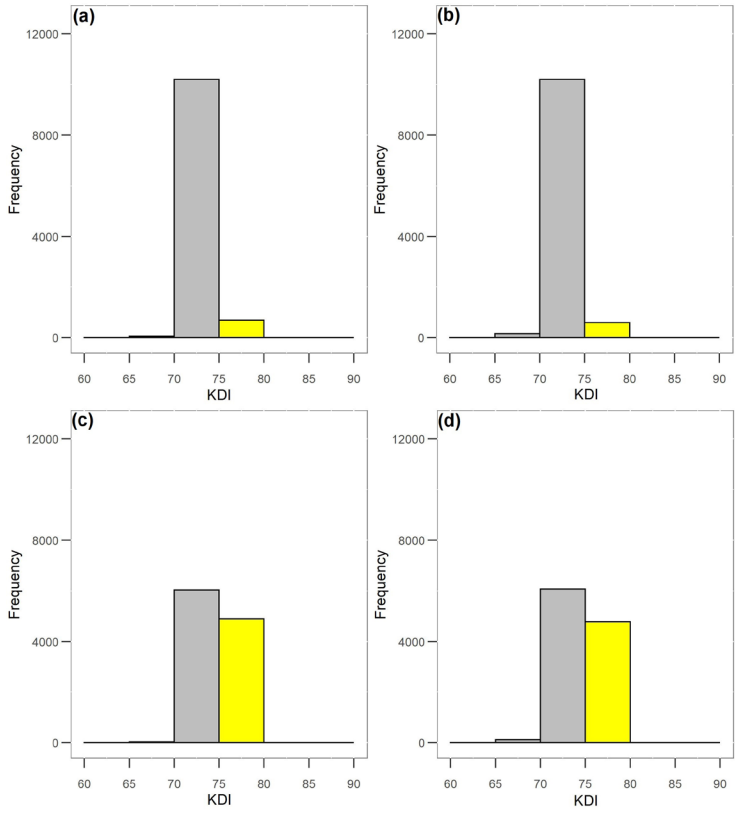

Figure 9. Histograms of the future scenarios of the daily KDI classification for the periods 2021-2050 according to scenarios A1B (a) and A2 (b), and 2051-2080 for scenarios A1B (c) and A2 (d), from the results of the models for Area 02. The gray color indicates the comfortable range, while yellow represents the uncomfortable range by heat.

CONCLUSIONS

In this study, future scenarios of climate change were used to evaluate the future trend of an index that measures the degree of human thermal comfort/discomfort with respect to the environment, by resorting to data sets of different sorts of variables, such as average temperature, dew point and the KDI.

In light of a scenario of long-term rainfall decline between 2021 and 2080, as well as temperature climb, three areas of the Northeast of Brazil (NEB) were analyzed: Area 01, the northernmost region, Area 02, comprising the eastern sector, and Area 03, which encompasses the central and western parts of the NEB. The models simulated well the KDI values for the reference period 1961-1990, also benefiting from the success in the employment of Multiple Linear Regression to obtain the relative humidity and consequent dew point data, which are indispensable for calculating the index.

For the three areas and for both scenarios (A1B and A2), the projections present a significant increase in the percentage of days with discomfort by heat. Regarding Area 01, the few occurrences of days still classified as comfortable during 2021-2050 should decrease even more in the period 2051-2080. For Area 02, the period 2021-2050 is still expected to present a predominance of days with thermal comfort, albeit much less numerous than during the control period (1961-1990), and that should be totally overcome by the prevalence of days of discomfort by heat in the period 2051-2080. Finally, Area 03 is the one that should experience the greatest changes, owing to the fact that, in the reference period, the days with discomfort by heat did not exceed 1% of the total, a percentage that, according to the projections, will increase to approximately

7% (from an average of the two scenarios) in the period 2021-2050, eventually reaching 48% on average in the period 2051-2080.

Acknowledgments

The authors thanks the Coordenação de Aperfeiçoamento de Pessoal de Nível Superior (CAPES) for the financial support during the conception of this study.

REFERENCES

ALVES JMB, SILVA EM, SOMBRA SS, BARBOSA ACB, SANTOS ACS & LIRA MAT. 2017. Eventos Extremos Diários de Chuva no Nordeste do Brasil e Características Atmosféricas. Rev Bras Meteorol 32(2): 227-233.

ANDRÉ RGB, MARQUES VS, PINHEIRO FMA & FERRAUDO AS. 2008. Identificação de regiões pluviometricamente homogêneas no estado do Rio de Janeiro, utilizando-se valores mensais. Rev Bras Meteorol 23: 501-509.

BELLOUIN N, BOUCHER O, HAYWOOD J, JOHNSON C, JONES A, RAE J & WOODWARD S. 2007. Improved representation of aerosols for HadGEM2. Meteorological Office Hadley Centre, Technical Note 73.

BENISTON M. 2004. The 2003 heat wave in Europe: A shape of things to come? An analysis based on Swiss climatological data and model simulations. Geophys Res Lett 31: L0220. doi:10.1029/2003GL018857.

BERTHOUEX PM & BROWN LC. 2002. Statistics for Environmental Engineers, 2nd Edition, Lewis Publishers/CRC Press, Boca Raton, FL, 489 p.

BOMBARDI RJ & CARVALHO LMV. 2009. IPCC Global coupled climate model simulations of the South America Monsoon System. Clim Dyn 33: 893-916.

CARTER TR. 2007. General Guidelines on the use of scenario data for Climate Impact and Adaptation Assessment. Finnish Environmental Institute, Helsinki, Finland.

CAVALCANTI EP & MARIANO EB. 2016. Tendência do Vapor D'Água na Atmosfera Mediante Dados do NCEP/NCAR. Rev Bras Meteorol 31: 564-569.

CHOU SC ET AL. 2014. Assessment of Climate Change over South America under RCP 4.5 and 8.5 Downscaling Scenarios. Am J Clim Change 03: 512-527.

COFIÑO AS, SAN-MARTÍN & GUTIÉRREZ JM. 2007. A Web Portal for Regional Projection of Weather Forecast Using GRID Middleware. In: Shi Y, van Albada GD, Dongarra J and Sloot PMA (Eds). Computational Science - ICCS 2007. ICCS 2007. Lecture Notes in Computer Science, v 4489. Springer, Berlin, Heidelberg.

CORDEIRO ES, FEDOROVA N & LEVIT V. 2018. Synoptic and thermodynamic analysis of events with thunderstorms for alagoas state in a period of 15 years (1998-2012). Rev Bras Meteorol 33: 685-694.

COSTA RL, BAPTISTA GMM, GOMES HB, SILVA FDS, DA ROCHA JÚNIOR RL, SALVADOR MA & HERDIES DL. 2020. Analysis of climate extremes indices over northeast Brazil from 1961 to 2014. Weather Clim Extremes 28: 100254. https://doi.org/10.1016/j.wace.2020.100254.

COSTA RL, DE SOUZA EP & SILVA FDS. 2014. Aplicação de uma teoria termodinâmica no estudo de um Vórtice Ciclônico de Altos Níveis sobre o nordeste do Brasil. Rev Bras Meteorol 29: 96-104.

CUNHA APMA, TOMASELLA J, RIBEIRO-NETO GG, BROWN M, GARCIA SR, BRITO SB & CARVALHO MA. 2018. Changes in the spatial-temporal patterns of droughts in the Brazilian Northeast. Atmos Sci Lett 19(10): e855. https://doi.org/10.1002/asl.855.

DA ROCHA JÚNIOR RL, SILVA FDS, COSTA RL, GOMES HB, HERDIES DL, SILVA VPR & XAVIER AC. 2019. Analysis of the Space-Temporal Trends of Wet Conditions in the Different Rainy Seasons of Brazilian Northeast by Quantile Regression and Bootstrap Test. Geosciences 9: 457.

DA ROCHA JÚNIOR RL, SILVA FDS, COSTA RL, GOMES HB, PINTO DDC & HERDIES DL. 2020. Bivariate Assessment of Drought Return Periods and Frequency in Brazilian Northeast Using Joint Distribution by Copula Method. Geosciences 10: 135.

DE CARVALHO M, ÂNGELO V & OYAMA MD. 2013. Variabilidade da largura e intensidade da Zona de Convergência Intertropical atlântica: Aspectos observacionais. Rev Bras Meteorol 28: 305-316.

FANGER PO. 1970. Thermal comfort. Analysis and applications in environmental engineering. McGraw-Hill, New York.

FLATO G ET AL. 2013. Evaluation of climate models. In Climate Change 2013: The Physical Science Basis. Contribution of Working Group I to the Fifth Assessment Report of the Intergovernmental Panel on Climate Change.

FRANCHITO SH, REYES FERNANDEZ JP & PAREJA D. 2014. Surrogate Climate Change Scenario and Projections with a Regional Climate Model: Impact on the Aridity in South America. Am J Clim Change 3: 474-489.

FROTA AB & SCHIFFER SR. 2003. Manual de conforto térmico: arquitetura e urbanismo. 7ª ed., São Paulo: Studio Nobel, 243 p.

GABRIEL KMA & ENDLICHER WR. 2011. Urban and rural mortality rates during heat waves in Berlin and Brandenburg, Germany. Environ Pollut 159: 2044-2050.

GASPARRINI A ET AL. 2015a. Temporal variation in heat-mortality associations: a multicountry study. Environ Health Perspect 123: 1200-1207.

GASPARRINI A ET AL. 2015b. Mortality risk attributable to high and low ambient temperature: a multicounty observational study. Lancet 386: 369-375.

GIVONI B. 1976. Man, climate and architecture. Van Nostrand Reinhold Company, London.

GOBO JPA & GALVANI E. 2012. Aplicação do Índice de temperatura efetiva com vento (TEV) nos estudos de conforto térmico para o estado do Rio Grande do Sul. Rev Geonorte 1(5): 403-413.

GOMES HB, AMBRIZZI T, DA SILVA BFP, HODGES K, DIAS PLS, HERDIES DL, SILVA MCL & GOMES HB. 2019. Climatology of easterly wave disturbances over the tropical South Atlantic. Clim Dyn 53: 1393-1411.

GOMES HB, AMBRIZZI T, HERDIES DL, HODGES K & DA SILVA BFP. 2015. Easterly Wave Disturbances over Northeast Brazil: An Observational Analysis. Adv Meteorol 2015: 176238.

GUIMARÃES SO, COSTA AA, VASCONCELOS JÚNIOR FC, SILVA EM, SALES DC, ARAÚJO JÚNIOR LM & SOUZA SG. 2016. Projeções de Mudanças Climáticas sobre o Nordeste Brasileiro dos Modelos do CMIP5 e do CORDEX. Rev Bras Meteorol 31(3): 337-365.

GUIRGUIS K, GERSHUNOV A, CAYAN DR & PIERCE DW. 2018. Heat wave probability in the changing climate of the Southwest US. Clim Dyn 50: 3853-3864.

GUO Y, BARNETT AG, PAN X, YU W & TONG S. 2011. The impact of temperature on mortality in Tianjin, China: a case-crossover design with a distributed lag nonlinear model. Environ Health Perspect 119: 1719-1725.

GUO Y ET AL. 2014. Global variation in the effects of ambient temperature on mortality: a systematic evaluation. Epidemiology 25: 781-789.

GUTIÉRREZ JM, SAN-MARTIN D, BRANDS S, MANZANAS R & HERRERA S. 2013. Reassessing statistical downscaling techniques for their robust application under climate change conditions. J Clim 26: 171-188.

HARTMANN DL ET AL. 2013. Observations: Atmosphere and Surface. In The Physical Science Basis. Contribution of Working Group I to the Fifth Assessment Report of the Intergovernmental Panel on Climate Change, p. 159-254.

HERVADA-SALA C & JARAUTA-BRAGULAT E. 2004. A program to perform Ward's clustering method on several regionalized variables. Comput Geosci 30: 881-886.

HUNT BG. 2007. A Climatology of Heat Waves from a Multimillennial Simulation. J Clim 20: 3802-3821.

IBGE. 2017. Censo Agro 2017. Disponível em https://www.ibge.gov.br/estatisticasnovoportal/economicas/agricultura-e-pecuaria/21814-2017-censoagropecuario.html?=&t=o-que-e. Acessado em 20.06.2018

IPCC. 2007. The physical science basis. Contribution of working group I to the fourth assessment Report of the IPCC. Cambridge University. Press, Cambridge.

IPCC. 2013. Working Group I Contribution to the IPCC Fifth Assessment Report AR5., Climate Change 2013: The Physical Science Basis. Intergovernmental Panel on Climate Change, Geneva, Switzerland.

ISHIZAKI N, DAIRAKU K, KUSAKA H, NAKAEGAWA T & TAKAYABU I. 2012. An Attempt to Estimate of Probabilistic Regional Climate Analogue in a Warmer Japan. J Meteorol Soc Japan 90B: 65-74.

KAYANO MT & ANDREOLI RV. 2004. Decadal variability of northern northeast Brazil rainfall and its relation to tropical sea surface temperature and global sea level pressure anomalies. J Geophys Res 109: C11.

KAYANO MT & CAPISTRANO VP. 2014. How the Atlantic Multidecadal Oscillation (AMO) modifies the ENSO influence on the South American rainfall. Int J Climatol 34: 162-178.

KOPF S, HA-DUONG M & HALLEGATTE S. 2008. Using maps of city analogues to display and interpret climate change scenarios and their uncertainty. Nat Hazards Earth Syst Sci 8: 905-918.

KOUSKY VE. 1979. Frontal influences on Northeast Brazil. Mont Weather Rev 107(9): 1140-1153.

KOUSKY VE & GAN MA. 1981. Upper Tropospheric Cyclonic Vortices in the Tropical South Atlantic. Tellus 33: 538-551.

KOUSKY VE & KAYANO MT. 1994. Principal modes of outgoing longwave radiation and 250mb circulation for the South American sector. J Clim 7: 1131-1143.

LEE H, HOLST J & MAYER H. 2013. Modification of human biometeorologically significant radiation flux densities by shading as local method to mitigate heat stress in summer within urban street canyons. Adv Meteorol 38: 1-13. doi:10.1155/2013/312572.

MARAUN D ET AL. 2010. Precipitation downscaling under climate change: recent developments to bridge the gap

between dynamical models and the end user. Rev Geophys 48: 1-38.

MARENGO JA, ALVES LM, ALVALÁ RCS, CUNHA APMA, BRITO SSB & MORAES OLL. 2018. Climatic characteristics of the 2010–2016 drought in the semiarid Northeast Brazil region. An Acad Bras Cienc 90: 1973-1985.

MARENGO JA, TORRES RR & ALVES LM. 2016. Drought in Northeast Brazilpast, present, and future. Theor Appl Climatol 129: 1189-1200.

MARSLAND SJ, HAAK H, JUNGCLAUS JH, LATIF M & ROESKE F. 2003. The Max-Planck-Institute global ocean/sea ice model with orthogonal curvilinear coordinates. Ocean Model 5: 91-127.

MARTINS ESPR, COELHO CAS, HAARSMA R, OTTO FEL, KING AD, VAN OLDENBORGH GJ, KEW S, PHILIP S, JÚNIOR FCV & CULLEN H. 2018. A multimethod attribution analysis of the prolonged northeast Brazil hydrometeorological drought (2012-16). Bull Am Meteorol Soc 99: 65-69.

MEEHL GA & TEBALDI C. 2004. More intense, more frequent, and longer lasting heat waves in the 21st century. Science 305: 994-997.

MIMMACK GM, MASON SJ & GALPIN JS. 2001. Choice of distance matrices in cluster analysis: defining regions. J Clim 14: 2790-2797.

MOLION LCB & LUCIO PS. 2013. A Note on Pacific Decadal Oscillation, El Nino Southern Oscillation, Atlantic Multidecadal Oscillation and the Intertropical Front in Sahel, Africa. Atm Clim Science 03: 269-274.

MOURA AD & SHUKLA J. 1981. On the dynamics of droughts in northeast Brazil: Observations, theory and numerical experiments with a general circulation model. J Atm Science 38: 2653-2675.

NÓBREGA RS & LEMOS TVS. 2011. O microclima e o (des) conforto térmico em ambientes abertos na cidade do recife. Rev Geog 28(1): 93-109.

ONO HSP & KAWAMURA T. 1991. Sensible climates in monsoon Asia. Int J Biometeorol 35: 39-47.

PERES LF, LUCENA AJ, FILHO OCR & FRANÇA JRA. 2018. The urban heat island in Rio de Janeiro, Brazil, in the last 30 years using remote sensing data. Int J Appl Earth Obs 64: 104-116.

RADDATZ TJ, REICK CH, KNORR W, KATTGE J, ROECKNER E, SCHNUR R, SCHNITZLER KG, WETZEL P & JUNGCLAUS J. 2007. Will the tropical land biosphere dominate the climate-carbon cycle feedback during the twenty first century? Clim Dyn 29: 565-574.

RASKIN P, MONKS F, RIBEIRO T, VAN VUUREN DP & ZUREK M. 2005. Global scenarios in historical perspective. In: Carpenter S and Pingali P (Eds). Millennium ecosystem assessment - scenarios assessment. Island Press, Washington.

SALES DC, COSTA AA, SILVA EM, VASCONCELOS JÚNIOR FC, CAVALCANTE AMB, MEDEIROS SS, MARIN AMP, GUIMARÃES SO, ARAÚJO JÚNIOR LM & PEREIRA JMR. 2015. Projeções de Mudanças na Precipitação e Temperatura no Nordeste Brasileiro Utilizando a Técnica de Downscaling Dinâmico. Rev Bras Meteorol 30(4): 435-456.

SALVIANO MF, GROPPO JD & PELLEGRINO GQ. 2016. Análise de Tendências em Dados de Precipitação e Temperatura no Brasil. Rev Bras Meteorol 31(1): 64-73.

SAMPAIO CAP, TEREZO RF, ROSA TO, BURIGO MC & ANDRADE LB. 2018. Similitude and Thermal Performance on Non-Conventional Roofs. Eng Agrícola 38(1): 7-12.

SANTOS JB, AMORIM RFC & CAVALCANTE LPA. 2014. Análise do conforto térmico humano no município de Arapiraca – Alagoas, utilizando Software MATLAB. Rev Bras Geog Física 07(05): 939-948.

SANTOS JS, SILVA VPR, LIMA ERV, ARAÚJO LE & COSTA ADL. 2012. Campo Térmico Urbano e a sua Relação com o Uso e Cobertura do Solo em Cidade Tropical Úmida. Rev Bras Geog Física 05(03): 540-557.

SCHÄR C, VIDALE PL, LÜTHI D, FREI C, HÄBERLI C, LINIGER MA & APPENZELLER C. 2004. The role of increasing temperature variability in European summer heat waves. Nature 427: 332-336.

SERVAIN J. 1991. Simple climatic indices for the tropical Atlantic Ocean and some applications. J Geophys Res 96: 137-146.

SERVAIN J, WAINER I, AYINA HL & ROQUET H. 2000. The Relationship Between the Simulated Climatic Variability Modes of the Tropical Atlantic. Int J Climatol 20: 939-953.

SILVA IR, NEDEL AS, MARQUES JRQ & NOLASCO JÚNIOR LR. 2018. Excess of children's outpatient consultations due to asthma and bronchitis and the association between meteorological variables in Canoas City, Southern Brazil. Int J Biometeorol 63(11): 1517-1524. doi: 10.1007/s00484-018-1650-z.

SILVA VBS, KOUSKY VE, SILVA FDS, SALVADOR MA & ARAVEQUIA JA. 2013. The 2012 severe drought over Northeast Brazil. Bull Am Meteorol Soc 94: 162.

SRES - EMISSIONS SCENARIOS. 2010. A Special Report of IPCC Working Group III. Published for the Intergovernmental Panel on Climate Change, ISBN: 92-9169-113-5.

STOTT PA, STONE DA & ALLEN MR. 2004. Human contribution to the European heat wave of 2003. Nature 432: 610-614.

THORSSON S ET AL. 2017. Present and projected future mean radiant temperature for three European cities. Int J Biometeorol 61: 1531-1543.

THORSSON S, ROCKLÖV J, KONARSKA J, LINDBERG F, HOLMER B, DOUSSET B & RAYNER D. 2014. Mean radiant temperature-a predictor of heat related mortality. Urban Clim 10: 332-345.

TIMBAL B & JONES DA. 2008. Future projections of winter rainfall in southeast Australia using a statistical downscaling technique. Clim Change 86(1-2): 165-187.

TRIGO RM, GARCIA-HERRERA R, DIAZ J, TRIGO IF & VALENTE MA. 2005. How exceptional was the early August 2003 heat wave in France. Geophys Res Lett 32: L10701. doi: 10.1029/2005GL022410.

VAN DEN DOOL HM. 1994. Searching for analogues, how long must one wait? Tellus 46A: 314-324.

VERGOLINO JR & DANTAS M. 2005. Os determinantes do processo de urbanização da região Nordeste do Brasil: 1970-1996. Economia 31: 7-33.

WILBY RL & DAWSON CW. 2004. SDSM 4.1 - A decision support tool for the assessment of regional climate change impacts. Environment Agency of England and Wales, Nottingham.

WILBY RL & DAWSON CW. 2013. The Statistical DownScaling Model: insights from one decade of application. Int J Climatol 33: 1707-1719.

WILBY RL, DAWSON CW & BARROW EM. 2002. SDSM - A decision support tool for the assessment of regional climate change impacts. Environ Modell Softw 17: 147-159.

WILBY RL & FOWLER HJ. 2010. Regional climate downscaling. In Modelling the Impact of Climate Change on Water Resources. Fung CF, Lopez A and New M (Eds). Wiley-Blackwell Publishing: Chichester.

WILBY RL & WIGLEY TML. 1997. Downscaling general circulation model output: a review of methods and limitations. Prog Phys Geogr 21: 530-548.

WILKS DS. 2011. Statistical Methods in the Atmospheric Sciences. Elsevier/Academic Press, Amsterdam and Boston, MA, 704 p.

ŽAGAR N, SKOK G & TRIBBIA J. 2011. Climatology of the ITCZ derived from ERA Interim reanalyses. J Geophys Res 116: D15103. doi:10.1029/2011JD015695.

ZORITA E, HUGHES JP, LETTENMAIER DP & VON STORCH H. 1995. Stochastic characterization of regional circulation patterns for climate model diagnosis and estimation of local precipitation. J Clim 8: 1023-1042.

ZORITA E & VON STORCH H. 1999. The analog method as a simple statistical downscaling technique: Comparison with more complicated methods. J Clim 12(8): 2474-2489.

How to cite

COSTA RL, BAPTISTA GMM, GOMES HB, SILVA FDS, DA ROCHA JÚNIOR RL & NEDEL AS. 2021. Analysis of future climate scenarios for northeastern Brazil and implications for human thermal comfort. An Acad Bras Cienc 93: e20190651. DOI 10.1590/0001-3765202120190651.

Manuscript received on June 7, 2019;
accepted for publication on May 17, 2020

RAFAELA L. COSTA[1]
https://orcid.org/0000-0002-8298-5901

GUSTAVO M.M. BAPTISTA[2]
https://orcid.org/0000-0002-1973-2725

HELIOFÁBIO B. GOMES[1]
https://orcid.org/0000-0003-1790-2505

FABRÍCIO D.S. SILVA[1]
https://orcid.org/0000-0002-3185-6413

RODRIGO L. DA ROCHA JÚNIOR[1]
https://orcid.org/0000-0003-4654-8947

ANDERSON S. NEDEL[3]
https://orcid.org/0000-0001-5456-6139

[1]Universidade Federal de Alagoas, Instituto de Ciências Atmosférica, Av. Lourival Melo Mota, s/n, Tabuleiro do Martins, 57072-900 Maceió, AL, Brazil

[2]Universidade de Brasília, Instituto de Geociências, Campus Darcy Ribeiro, ICC, Asa Central, 70910-900 Brasília, DF, Brazil

[3]Universidade Federal da Fronteira Sul, Campus Cerro Largo, Rua Jacob Reinaldo Haupenthal, 1580, São Pedro, 97900-000 Cerro Largo, RS, Brazil

Correspondence to: **Rafaela Lisboa Costa**
E-mail: rafaelalisboac@gmail.com

Author contributions

Rafaela Lisboa Costa: Conceptualization, formal analysis, methodology writing, supervision. Gustavo Macedo de Mello Baptista: Writing, formal analysis. Heliofábio Barros Gomes: Methodology, data curation, writing. Fabrício Daniel dos Santos Silva: Data processing, data curation, analysis. Rodrigo Lins da Rocha Júnior and Anderson Spohr Nedel: Methodology, analysis.